Journal of Minerals and Materials Characterization and Engineering, 2023, 11, 143-160
https://www.scirp.org/journal/jmmce
ISSN Online: 2327-4085
ISSN Print: 2327-4077

# Experimental and Numerical Study of Mechanical Behaviour of Fired Clay Bricks after Exposure to High Temperatures

**Jean Calvin Bidoung[1]*, Léon Arnaud Mpoung[1], Jean Aimé Mbey[2], Jean Raymond Lucien Meva'a[1]**

[1]Laboratory of Civil Engineering and Mechanics, National Advanced School of Engineering of Yaoundé, University of Yaoundé 1, Yaoundé, Cameroon
[2]Laboratory of Applied Inorganic Chemistry, Department of Inorganic Chemistry, University of Yaoundé 1, Yaoundé, Cameroon
Email: *bidoung@yahoo.com

**How to cite this paper:** Bidoung, J.C., Mpoung, L.A., Mbey, J.A. and Meva'a, J.R.L. (2023) Experimental and Numerical Study of Mechanical Behaviour of Fired Clay Bricks after Exposure to High Temperatures. *Journal of Minerals and Materials Characterization and Engineering*, **11**, 143-160.
https://doi.org/10.4236/jmmce.2023.115012

**Received:** July 25, 2023
**Accepted:** September 5, 2023
**Published:** September 8, 2023



## Abstract

This paper reports the modeling of residual compressive strength of fired clay bricks submitted to elevated temperature. Five formulations were used and the explored temperatures were 95˚C, 200˚C, 550˚C, 700˚C and 950˚C. The stress–strain relationships and the mechanical properties (including Young's modulus and compressive strength) were assessed using a uniaxial compressive strength machine. A proposed model equation was established and found satisfying. The elastic modulus was evaluated and tested with one existing model together with two proposed models. The proposed model was both satisfying and even more precise than the existing one. The overall results show that the effect of temperature on the mechanical properties of clays can be accurately described through the definition of thermal damage using elastic modulus.

## Keywords

Clay Bricks, Modeling, Stress-Strain Equations, Compressive Strength, Young's Modulus

## 1. Introduction

Fire stands as one of the major risks to which buildings are exposed [1]-[7]. Among the building materials existing in the construction sector, concrete is increasingly used due to its service duration which depends on several factors such as its composition, its properties in particular compressive or splitting tensile strength and despite of short time of exposure to high temperature consequences on its performance [8]. Therefore, its fire behaviour and the one of the newly

developed one is a research field of interest, in which studies have been made on the residual mechanical properties after exposure to elevated temperatures. This included compressive strength, splitting tensile strength, stress-strain and elastic modulus [9]-[24].

Clay bricks, although amongst the oldest material in construction, are widely spread and still subjected to many research works [25] [26] [27]. The reason for such interest is due to the low cost and availability of clays that are raw materials for brick making. In the case of developing countries, the valorization of such local resources is of interest for the promotion of quality and low cost housing. In order to have a good mastering of the building survey, assessing their mechanical behaviour after exposure to high temperatures remains a challenging field [28]. In addition, considering the variability of the raw materials used for brick making, it is also interesting to determine a general feature of the behaviour designed for bricks exposed to fire. The behaviour of building structural members is predictable using the material properties, cross-sectional properties and loading conditions, using computerized non-linear structural analysis techniques. This indicates that material properties and bricklaying can be also best described by their stress-strain relationship [25]-[30].

Clay bricks are used to resist compression and the knowledge of their compression behaviour is of interest for quality and safe buildings. To this end, the stress-strain behaviour of clay bricks is a compelling knowledge. In the literature, there is a lack of work dealing with the generation of the stress-strain behavior of masonry and its components after exposure to fire compared to other construction materials [31] [32] [33] [34] [35]. Given the similarity of concretes with clay bricks, there is a great interest in mastering the life cycle of buildings involving clay bricks by using stress-strain concrete model structure at ambient and elevated temperatures with available experimental results [36] [37]. In general, many of the reported studies are focused on the residual mechanical properties of clay bricks after exposure to elevated temperatures. Their description and modeling seem to attract research interests for a better understanding of their mechanical properties evolution. Their behavior need to be assessed, studies dealing with clay bricks are scarcely present in the literature [25] [28] [38] [39] [40] [41]. Not long ago, efforts were made by scientists to investigate the firing efficiency of bricklaying. The heat dependency of the appropriate mechanic characteristics (elastic modulus, crushing resistance, stress-strain approach in pressure, apex and final strain) for bricklaying and its constituents, into and following vulnerability to elevated heat was identified [25]. Heretofore, it was suggested the characteristic-heat relationships of mechanic deterioration for bricklaying [42] and its parts following elevated heat exposure through two temperatures 300˚C and 600˚C. A particular attention was given on both mechanic and thermal performances [28]. Inquiry proceeded on the progress of themselves geomorphological characteristics (micro level, water porousness, specific gravity) in line with heat exposition were exploited for a stronger understanding of the aforementioned characteristics of the tested material for three

warming-cool cycling under ambient temperature to 200˚C, 400˚C and 600˚C.

The present study stands as a contribution to evaluate fired clay bricks mechanical evolution upon exposure to high temperature. This information is of interest to estimate the material durability as exposed to thermal shock. A modeling of the stress-strain behaviour of these materials is proposed and compared to two reported models from the literature.

## 2. Materials and Methods

### 2.1. Experimental Investigation

The chemical and mineralogical compositions of the two clays selected Nsimalen (F0) and Etoa (F1), two localities around Yaounde (Cameroon), are given in Table 1 and Table 2 respectively.

The test briquettes were formulated as typical cubics of 4 × 4 × 4 cm according to ASTM C67 standard. Five formulations were adopted and are recapitulated in Table 3. The formulations mixing F1 and F0 are used to improve vitrification during sintering associated to illite content in F1 and to enhance refractoriness through the iron oxide content from F1.

For every formulation and for each temperature, a series of five specimens were used and the mean value from five tests was considered. Figure 1 summarizes the experimental investigation.

The compressive tests were carried out on a universal testing machine of 2000 kN to ASTM C67-80a standard. The linear modulus of elasticity, the invariable of Hooke's law is determined following Equation (1) [39].

Table 1. Chemical composition of F0.

| Chemical composition | | | | | | | | | | | |
|---|---|---|---|---|---|---|---|---|---|---|---|
| Element | $SiO_2$ | $Al_2O_3$ | $Fe_2O_3$ | $TiO_2$ | MnO | MgO | CaO | $NaO_2$ | $K_2O$ | $P_2O_5$ | LOI |
| wt% | 61.14 | 31.09 | 0.74 | 1.25 | 0.01 | 0.00 | 0.09 | 0.00 | 0.07 | 0.06 | 5.36 |

Table 2. Chemical and mineral compositions of F1 [43].

| Chemical composition of clay | | | | | | | | | | | | | |
|---|---|---|---|---|---|---|---|---|---|---|---|---|---|
| Element | $SiO_2$ | $Al_2O_3$ | $Fe_2O_3$ | $TiO_2$ | MgO | CaO | $K_2O$ | $Na_2O$ | $P_2O_5$ | $Mn_2O_3$ | BaO | $ZrO_2$ | LOI |
| wt% | 54.9 | 23.4 | 4.8 | 1.9 | 0.9 | 0.5 | 0.5 | 0.2 | 0.2 | 0.1 | 0.1 | 0.0 | 10.5 |
| Mineralogical composition of clay | | | | | | | | | | | | | |
| Element | Kaolinite | | Quartz | Geothite | | Rutile | | Gibsite | | Halloysite | | Feldspar | |
| %(mineral) | 47 | | 24.1 | 5.2 | | 3.4 | | 3.6 | | 4.0 | | 1.9 | |

Table 3. Formulation of the specimens.

| Formulations | F0 | F1 | F2 | F3 | F4 |
|---|---|---|---|---|---|
| F0:F1Proportion (w/w%) | 100:0 | 0:100 | 90:10 | 80:20 | 70:30 |

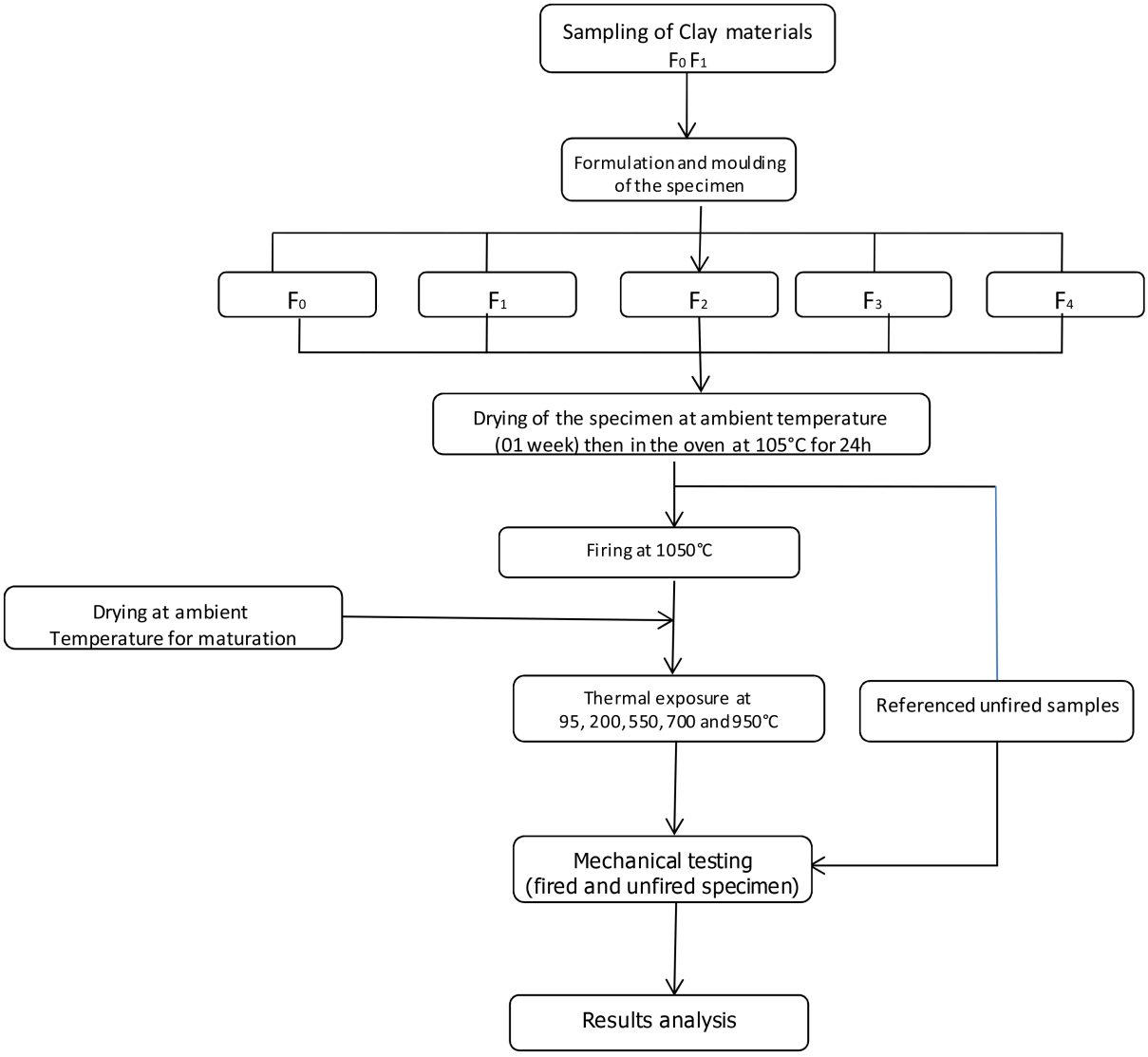


**Figure 1.** Experimental plan flow chart.

$$E = \frac{f_y - f_b}{\varepsilon_y - \varepsilon_b} \tag{1}$$

where:

- $f_y$ is the stress at the yield point (MPa);
- $\varepsilon_y$ is strain at the yield point;
- $f_b$ is the stress at the beginning of the linear zone (MPa);
- $\varepsilon_b$ is the strain at the beginning of the linear zone;
- $E$ is the linear modulus of elasticity (MPa).

## 2.2. Modeling of the Stress-Strain Relationships

To model the stress-strain relationship the Popovics' model ([36] [44]) and the generalized logistic equation were considered. Equation (2) is used assuming the same hypothesis stated by [44]. The relation given in Equation (2) and Equation

(3) stands for the complete stress-strain relationship:

$$\begin{cases} \dfrac{f_c}{f_c'} = \dfrac{\beta\left(\varepsilon/\varepsilon_c'\right)}{\beta - 1 + \left(\varepsilon/\varepsilon_c'\right)^{\beta}}, \quad f_c', \varepsilon_c', \beta, E_{it} \in R \\ \beta = \dfrac{1}{1 - \dfrac{f_c'}{\varepsilon_c' E_{it}}} \end{cases} \tag{2}$$

for $\beta \geq 1.0$ and $\varepsilon \leq \varepsilon_u$ where:

- $\beta$ is a material parameter that depends on the shape of the stress-strain curve.
- $f_c'$ is the maximum stress.
- $\varepsilon_c'$ is the strain corresponding to the maximum stress $f_c'$.
- $E_{it}$ is the slope at the origin or initial tangent modulus.

The following parameters $f_c'$, $\varepsilon_c'$ and $\beta$ or $E_{it}$ can be determined from compression tests with controlled strain rate. For design purposes, an ultimate strain $\varepsilon_u$ is specified to limit the degree of failure allowed in the bricks and

$$f_c = g + \frac{a}{b + ce^{-d(\varepsilon - e)}}, \quad a, b, c, d, e, g \in R \tag{3}$$

The nonlinear adjustment technique is made use for assessing the variables $a, b, c, d, e, g$. Excel solver was employed to elaborate these analytical modeling. An accurate way out was attained using a Newton-Raphson procedure. The correctness of the utmost suit model in this nonlinear retrogression assay established with experimental data relations is in accordance with the coefficient of determination $R^2$.

## 3. Results and Discussions

### 3.1. Compressive Strength

The bricks heated at the following temperatures 29˚C. 95˚C. 200˚C. 550˚C. 700˚C and 950˚C were submitted to compressive tests to determine the compressive strength. A model gives the numerical results of the compressive strength at the previously mentioned temperatures. These results are illustrated in **Figures 2-4**.

#### 3.1.1. Comparison of Experimental Results

The formulation F0 gives better mechanical performances than the formulation F1. Meanwhile, we obtain good compressive strengths after the substitution of the formulation F0 for the formulation F4 followed by the formulation F2.

This can be explained by the phase evolution and/or grain cohesion within the fired bricks. At lower temperature, the organization of moisture water within the porous matrix of the fired bricks may then increase the strength.

After 200˚C, this water is removed and the bonding forces and grain junction within the ceramics are affected, resulting in a fragile cohesion, which is more easily reduced. This might lead to the appearance of crack closure regions, particularly after thermal treatment [41].

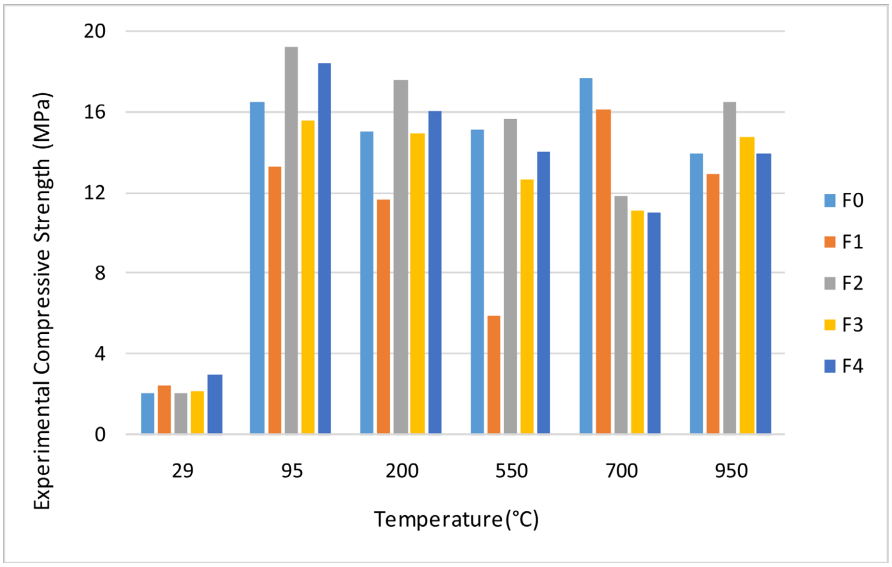


**Figure 2.** Experimental compressive strength of the various formulations after heating at different temperatures.

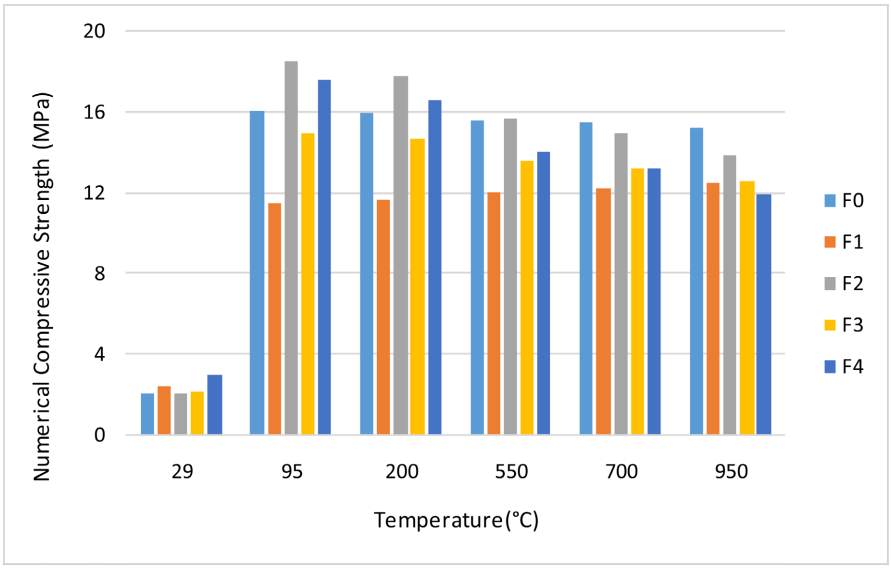


**Figure 3.** Numerical compressive strength of the various formulations after heating at different temperatures.

### 3.1.2. Comparison between Experimental and Numerical Results

The numerical results are given by Equation (4) obtained using the regression analysis. It is observed that all the formulations have the same relationships, suggesting a similarity in behavior likely due to mineral composition and proportion.

To assess the appropriateness of the matching of curves to the data, we used the coefficient of determination ($R^2$). It indicates that the suggested model gives a good approximation of the data. A comparison with the existing models [25] [28] [45] mainly the Russo's model shows many closed results for the different formulations, indicating that the proposed model is suitable.

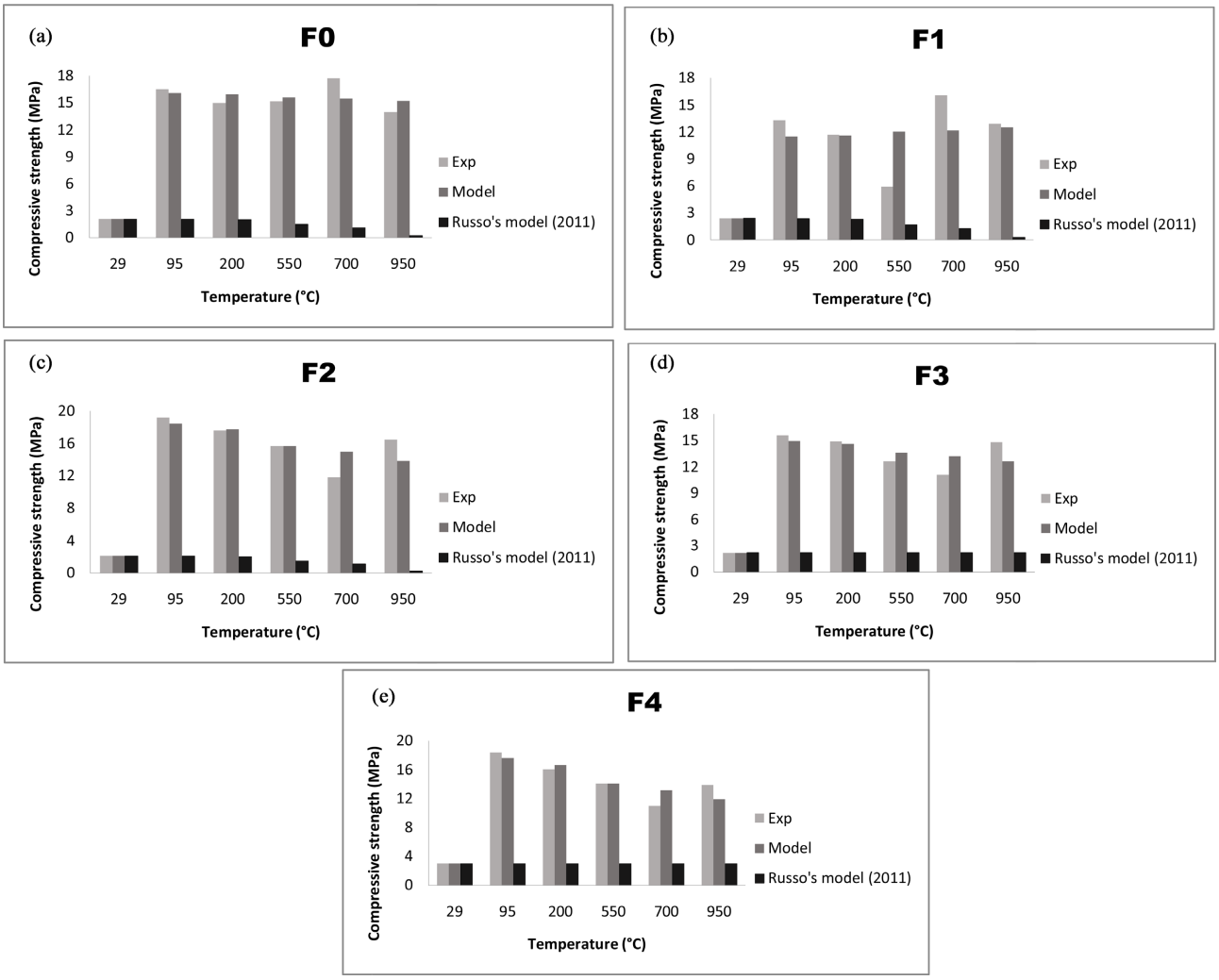


**Figure 4.** Experimental and numerical compressive strength after heating of the various formulations at different temperatures (a) F0; (b) F1; (c) F2; (d) F3; (e) F4.

We notice a variation from 0 to 24.19% (12.24 MPa) for the formulations F0 and F1 while the comparison between experimental and numerical results shows a variation from 0 to 26.75% (15 MPa) for the other formulations.

$$\frac{f'_{cT}}{f'_c(29^\circ\mathrm{C})} = \begin{cases} \dfrac{\tanh\left(-7.32\times10^{-2}T+1.992\right)}{-8.62\times10^{-6}T-0.129};\ R^2=0.95;\ \text{for F0} \\ \dfrac{\tanh\left(-7.5\times10^{-2}T+1.957\right)}{1.93\times10^{-5}T-0.21};\ R^2=0.58;\ \text{for F1} \\ \dfrac{\tanh\left(-7.3\times10^{-2}T+2.00073\right)}{-4.424\times10^{-5}T-0.1094};\ R^2=0.910;\ \text{for F2} \\ \dfrac{\tanh\left(-7.34\times10^{-2}T+1.984\right)}{-3.23\times10^{-5}T-0.144};\ R^2=0.916;\ \text{for F3} \\ \dfrac{\tanh\left(-7.34\times10^{-2}T+1.972\right)}{-9.52\times10^{-5}T-0.161};\ R^2=0.934;\ \text{for F4} \end{cases} \quad (4)$$

### 3.2. Elastic Modulus in Compression

Figures 5-7 give the various results of the Young' modulus. A model gives the numerical results.

#### 3.2.1. Comparison of Experimental Results

A rise of the elastic modulus at 95˚C, followed by a sudden drop up to 950˚C, is being observed in accordance with the previous observations [46]. It is seen that after a global increase at 200˚C, there is a decrease followed by an increase for all the formulations at 550˚C. The decrease is also observed at 700˚C and 950˚C except for F1 at 700˚C, F2 and F4 at 950˚C. This is probably due to the contraction of the clay specimens under thermal treatment and decrease in volume at 200˚C as water is being removed. The occurrence of thermal stress may lead to

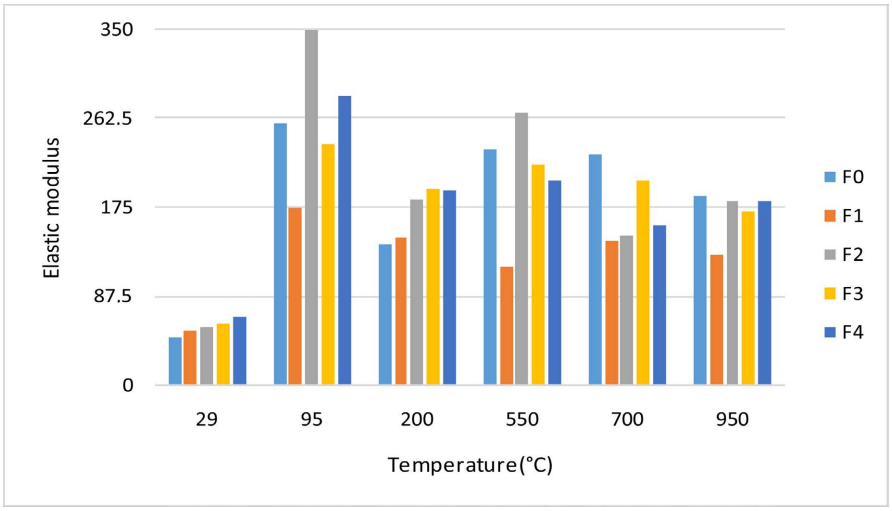


Figure 5. Experimental elastic modulus of the various formulations after heating at different temperatures.

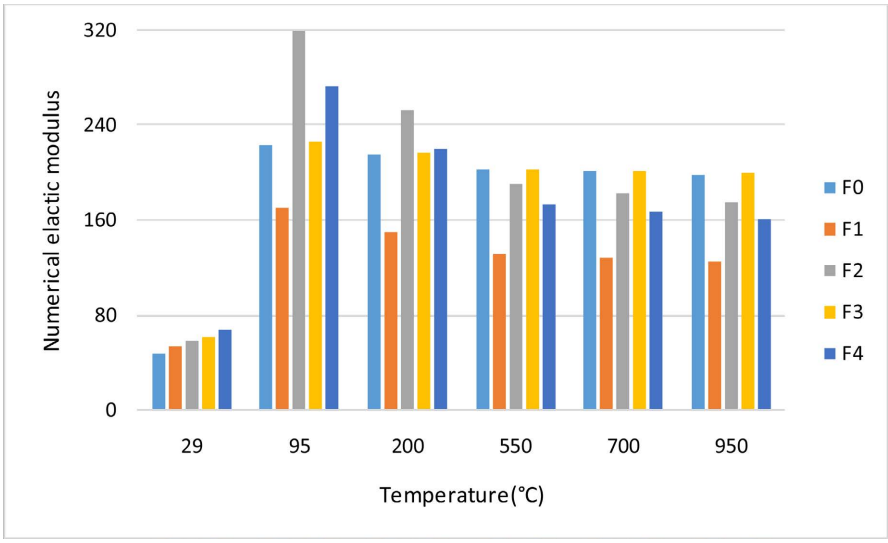


Figure 6. Numerical elastic modulus of the various formulations after heating at different temperatures.

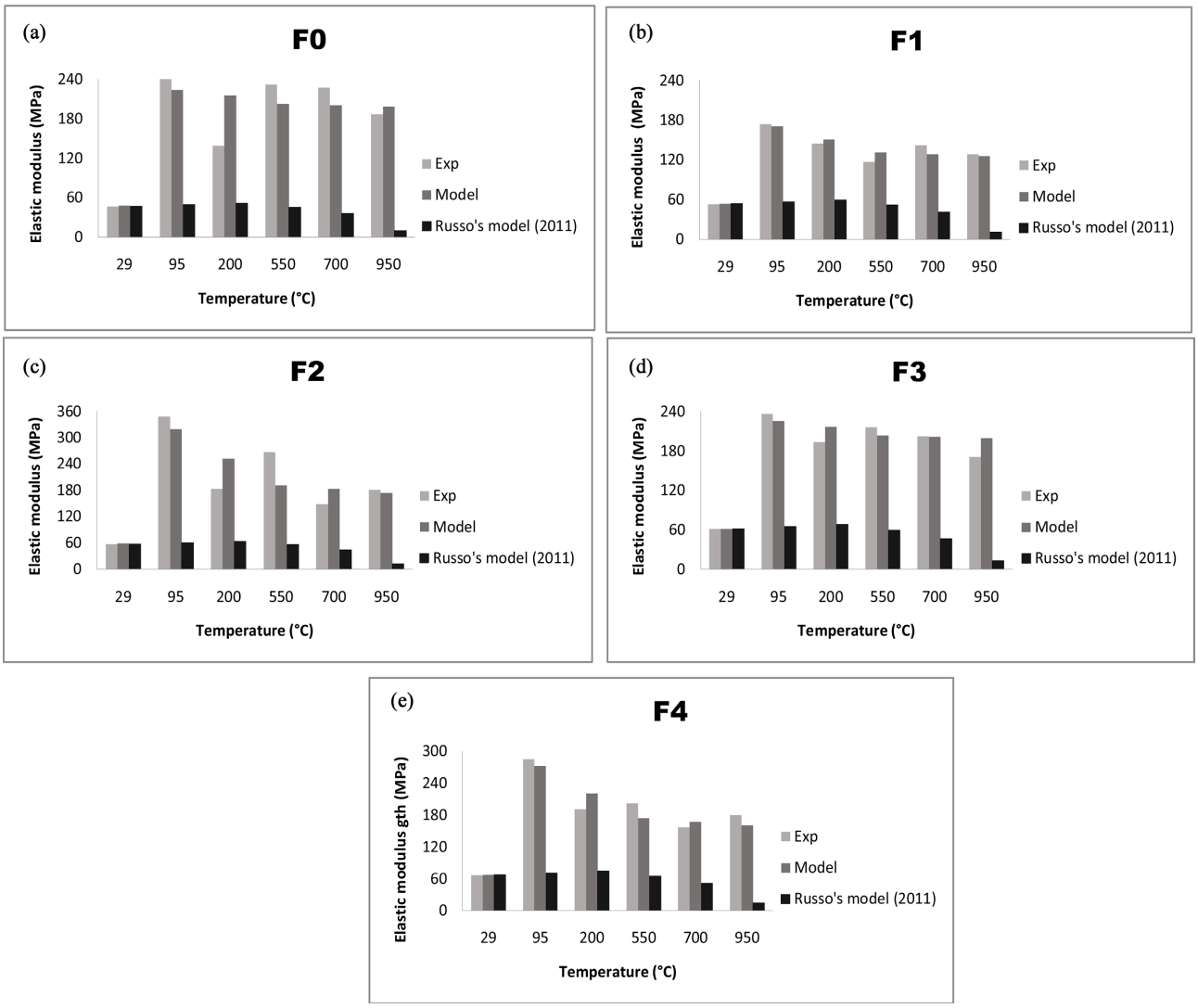


**Figure 7.** Experimental and numerical Elastic modulus after heating of the various formulations at different temperatures (a) F0; (b) F1; (c) F2; (d) F3; (e) F4.

the formation of thermal cracks at the boundaries of the grains [19]. Above 200˚C there is formation of intra-granular and inter-granular cracks after thermal treatment and brittle failure. That is why from 550˚C to 950˚C the elastic modulus decreases. The decrease of the elastic modulus with increasing temperature observed is associated to the damaging scheme of the materials. Increasing temperature may cause fractures, inducing strain that result in the lowering of the primary hardness [25].

### 3.2.2. Comparison of Experimental and Numerical Results

The use of the nonlinear fitting method leads to the relation of the compressive elastic modulus versus the temperature $T$, depicted in Equations (5).

$$\frac{E_{cT}}{E_c(29^{\circ}\mathrm{C})}=\begin{cases}-6.384\times10^{3}\left(\frac{1}{T}\right)^{2}+1.30\times10^{2}\frac{1}{T}+4.134;\ R^{2}=0.7131;\ \text{for F0}\\ -5.373\times10^{3}\left(\frac{1}{T}\right)^{2}+1.504\times10^{2}\frac{1}{T}+2.203;\ R^{2}=0.95;\ \text{for F1}\\ -1.373\times10^{4}\left(\frac{1}{T}\right)^{2}+4.273\times10^{2}\frac{1}{T}+2.6109;\ R^{2}=0.75;\ \text{for F2}\\ -4.709\times10^{3}\left(\frac{1}{T}\right)^{2}+1.00001\times10^{2}\frac{1}{T}+3.16;\ R^{2}=0.96;\ \text{for F3}\\ -9.071\times10^{3}\left(\frac{1}{T}\right)^{2}+2.806\times10^{2}\frac{1}{T}+2.12;\ R^{2}=0.924;\ \text{for F4}\end{cases} \quad (5)$$

As reported previously, the speculative progression modeling allows a two degree polynomial [28]. A comparative analysis with Russo's model with the previous statistics assessment scheme is made. It is observed that the Russo's model doesn't go beyond 600˚C and doesn't match the data closed to that temperature for all formulations while Equation (5) fit them well suggesting that it is more adequate.

### 3.3. Compressive Stress-Strain Curves

In Figures 8-10, the compressive stress-strain curves. The fitted curves and the validation of the suggested models at different temperatures are given respectively.

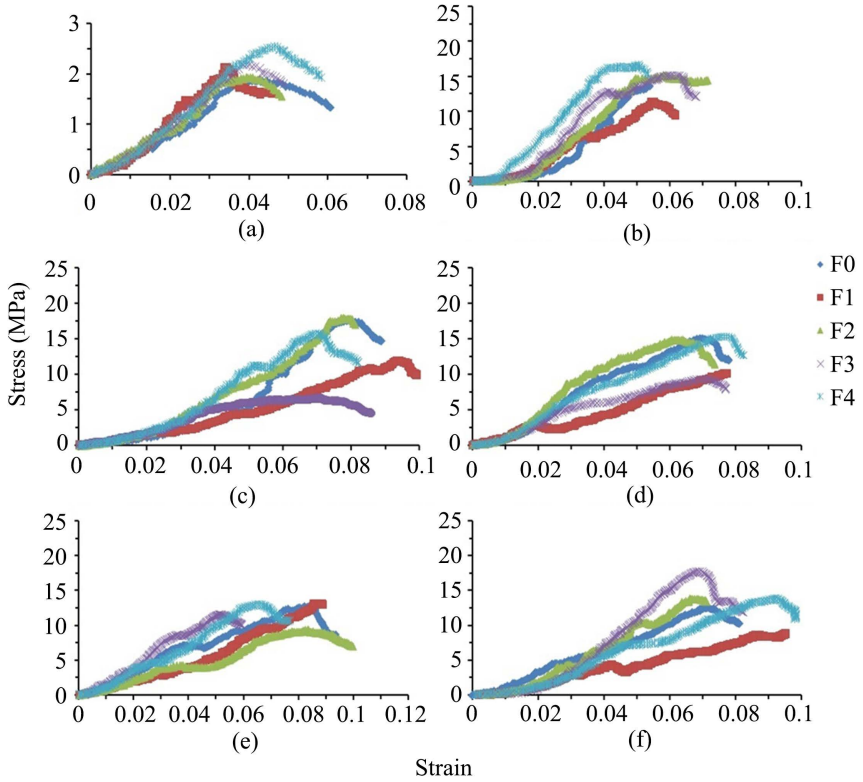


Figure 8. Stress-strain curves after heating of the various formulations at different temperatures (a) 29˚C; (b) 95˚C; (c) 200˚C; (d) 550˚C; (e) 700˚C; (f) 950˚C.

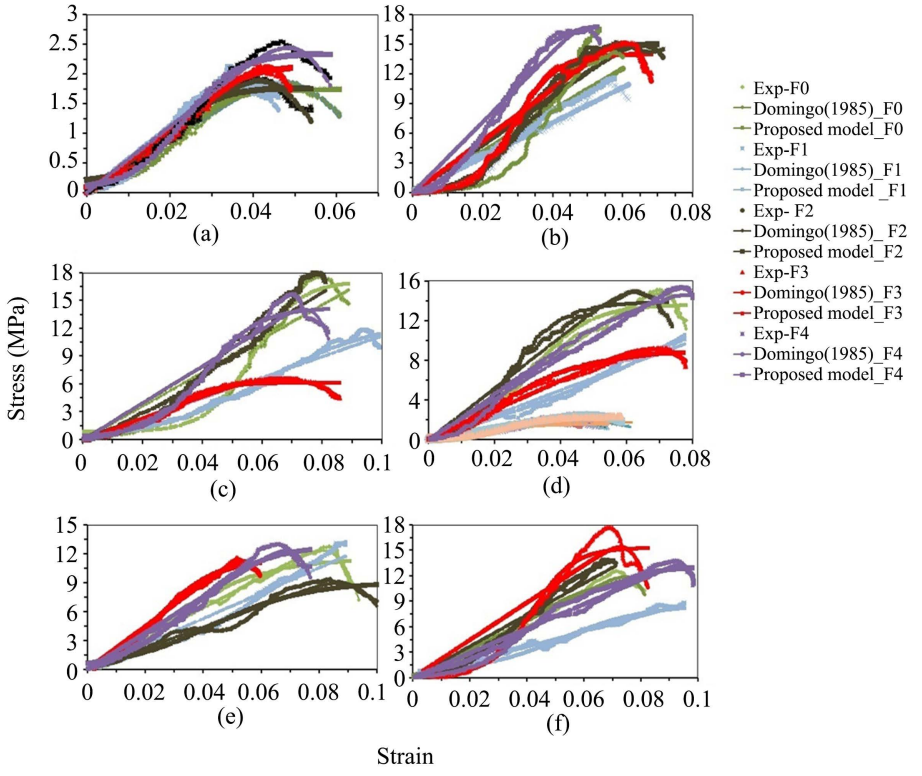


**Figure 9.** Test data and fitted stress-strain diagrams for different clays at different temperature (a) 29˚C; (b) 95˚C; (c) 200˚C; (d) 550˚C; (e) 700˚C; (f) 950˚C.

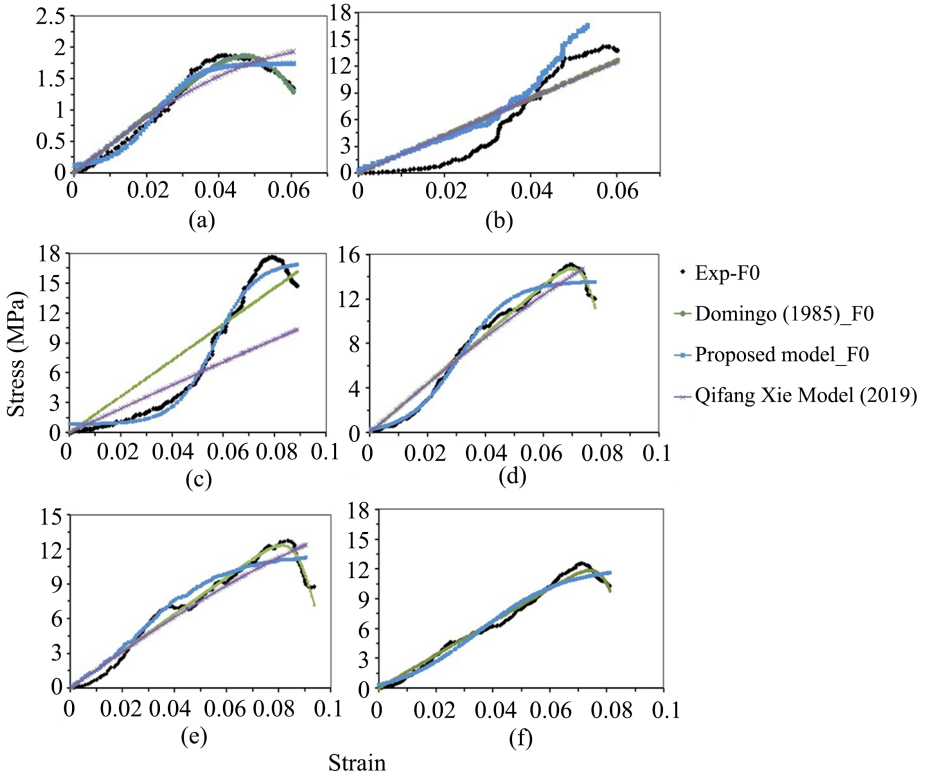


**Figure 10.** Comparison of the proposed stress-strain curves with other models. (a) 29˚C; (b) 95˚C; (c) 200˚C; (d) 550˚C; (e) 700˚C; (f) 950˚C.

#### 3.3.1. Comparison of Experimental Results

The stress-strain curves present an S-shaped form. From the various curves formulations three domains are observable [39]:

- a linear zone which might be caused by the effect of platens and material plasticity for all temperatures;
- a linear area revealed a rougher and furthermore straight line until the yielding stress following the Hooke law.
- a non-rectilinear behavior until the peak and just after it passing from elasticity to plasticity behavior occurs;

Brittleness and ductility can be linked to the density of thermal cracks and the last one to the closure of open microcracks [47]. As the temperature increases, the nonlinear deformation is getting more precise because higher temperature exposure caused the thermal cracks. Then, the elastic deformation is the most important feature in the linear portion of the stress-strain curves. As the deformation increases, the stress-strain curves live in linear behavior indicating the yielding of the samples, and then the samples reach the peak strength and enter the post peak deformation stage. As the temperature increases, the samples fail more slowly after the peak strength with the deformation increase.

Assuming the following rock characteristics suggested for clay enables us to explain the failure observed [48]:

- natural heterogeneous material;
- inequality of strength for various regions;
- initiation of cracks as the applied stress concentration exceeds the strength of the local material;
- occurrence of local cracking;
- transfer of stress concentration to tip of the crack;
- continuous propagation of failure in the region.

At room temperature, clay is hard but easily broken. We observe at the surface splitting failure and cracks which cause a representative brittle post-peak deformation. The same remarks are made at 200˚C. However, as the samples contain thermally induced cracks, the fracture development process might affect them mainly at 700˚C - 950˚C with small cracks due to smaller thermal damage before compression. On the other hand, at 950˚C, the final failure mode is different from the previous one, at the previous temperatures. Only shear failure is observed because of the bigger thermal damage before compression.

#### 3.3.2. Comparison of Experimental and Numerical Results

A closed match between the fitted curves and the experimental one is observed. This observation indicates that Equation (3) is usable to depict the clay brick compressive stress-strain relationships. It turns out that the modeling of fired clay brick stress-strain relationship is comparable to concrete behavior [48]. To validate the suggested models, a comparative analysis is made with cooling and heating experimental curves at various temperatures, the QifangXie model [8]. The proposed model fits the experimental stress-strain curves well in compari-

son with the two mentioned models for all formulations. Therefore, only the results of the formulation F0 are presented in Fig. 10.

### 3.3.3. Characteristic Parameters of the Constitutive Law

Experimental data suggests that the parameter $\beta$ varies none linearly in accordance with the temperature. Subsequently, the statistical analysis carried out yields the relations summarized in Table 4 for the various formulations.

Table 4 shows that the parameter $\beta$ for the various formulations F0, F2, F3 and F4 can be estimated by the same relationship with the following coefficient of determination $R^2 > 0.65$ indicating a good dependence between $\beta$ and $T$. It can also be noticed that, another expression can be used to estimate β for the formulation F4, although they have the same coefficient of determination ($R^2$ = 0.7063). In addition, no relationship was found to estimate the relation between $\beta$ and T for the formulation F1 because $R^2 < 0.6$. Table 5 gives an approximation of the parameters $a$, $b$, $c$, $d$, $e$ and $g$ with respect to the temperature for all formulations, with a coefficient of determination $R^2 > 0.999$, suggesting good agreement between each parameter and T.

## 4. Conclusions

The aim of this paper is to study the mechanical behavior of various clay-based formulations heated from 29˚C to 950˚C, from an experimental and numerical point of view. It appears that the substitution of the formulation F0 leads to good mechanical properties. This confirms the possibility to use the other formulations observed. The numerical study enables us to notice a maximum difference up to 26%. This difference is attributed to the brittleness of the clay and thermal stress occurrence. The suggested compressive stress-strain model fits fired clays bricks compressive experimental data at elevated temperatures which affect the shape of the stress-strain curve and its parameters. Proposed models for the compressive strength and elastic modulus as a function of the heating

Table 4. Expression of parameter β for different formulations.

| Formulation | Model Equation | $R^2$ |
|---|---|---|
| F0 | $\frac{\beta(T)}{\beta(29^\circ\mathrm{C})} = 0.842e^{0.0238T}\cos 0.001247T$ | 0.9562 |
| F2 | $\frac{\beta(T)}{\beta(29^\circ\mathrm{C})} = -1.4179e^{0.0000322T}\cos 0.9637T$ | 0.6853 |
| F3 | $\frac{\beta(T)}{\beta(29^\circ\mathrm{C})} = -1.0978e^{0.000876T}\cos 0.9637T$ | 0.8302 |
| F4 | $\frac{\beta(T)}{\beta(29^\circ\mathrm{C})} = 1.2511e^{0.01346T}\cos 1.273510^{-9}T$ | 0.7063 |
| | $\frac{\beta(T)}{\beta(29^\circ\mathrm{C})} = 1.2511e^{0.01346T}$ | 0.7063 |

**Table 5.** Expression of parameters a. b. c. d. e. and g for different formulations.

| Formulation | Model Equation | $R^2$ |
|---|---|---|
| F0 | $\begin{cases} a=-4\times10^{-11}T^5+10^{-7}T^4-9\times10^{-5}T^3+3.6\times10^{-2}T^2-5.684T+286.5 \\ b=-3\times10^{-11}T^5+6\times10^{-8}T^4-6\times10^{-5}T^3+2.22\times10^{-2}T^2-3.512T+175.8 \\ c=-1\times10^{-12}T^5+3\times10^{-9}T^4-2\times10^{-6}T^3-0.06T+2.257 \\ d=-9\times10^{-11}T^5+2\times10^{-7}T^4+6.8\times10^{-2}T^2-9.107T+389.55 \\ e=2\times10^{-12}T^5-5\times10^{-9}T^4+5\times10^{-6}T^3-10^{-3}T^2+0.2T+4.519 \\ g=-2\times10^{-11}T^5+4\times10^{-8}T^4-3\times10^{-5}T^3+1.1\times10^{-2}T^2-1.48T+33.89 \end{cases}$ | 0.9999 |
| F1 | $\begin{cases} a=-2\times10^{-11}T^5+6\times10^{-8}T^4-5\times10^{-5}T^3+2.0\times10^{-2}T^2-3.341T+179.1 \\ b=-2\times10^{-11}T^5+4\times10^{-8}T^4-3\times10^{-5}T^3+1.3\times10^{-2}T^2-2.077T+104.8 \\ c=-1\times10^{-12}T^5+2\times10^{-9}T^4-2\times10^{-6}T^3-0.044T+0.963 \\ d=-8\times10^{-11}T^5-2\times10^{-7}T^4+6.3\times10^{-2}T^2-9.177T+444.1 \\ e=2\times10^{-11}T^4-4\times10^{-8}T^3+2\times10^{-5}T^2-3\times10^{-3}T+0.136 \\ g=-2\times10^{-11}T^5+6\times10^{-8}T^4-5\times10^{-5}T^3+1.6\times10^{-2}T^2-2.089T+47.55 \end{cases}$ | 0.9999 |
| F2 | $\begin{cases} a=4\times10^{-10}T^4-8\times10^{-7}T^3-0.176T+17.21 \\ b=-2\times10^{-12}T^5+6\times10^{-9}T^4-5\times10^{-6}T^3+2\times10^{-3}T^2-0.312T+16.06 \\ c=-9\times10^{-11}T^4-2\times10^{-7}T^3+0.034T-0.918 \\ d=6\times10^{-9}T^4-1\times10^{-5}T^3+9\times10^{-3}T^2-2.379T+258.1 \\ e=10^{-12}T^4-4\times10^{-9}T^3-4\times10^{-6}T^2-0.001T+0.096 \\ g=9\times10^{-13}T^5-2\times10^{-9}T^4+2\times10^{-6}T^3+0.043T-0.641 \end{cases}$ | 0.9999 |
| F3 | $\begin{cases} a=-4\times10^{-12}T^5+9\times10^{-9}T^4-8\times10^{-6}T^3+3\times10^{-3}T^2-0.462T+25.16 \\ b=-2\times10^{-12}T^5+5\times10^{-9}T^4-4\times10^{-6}T^3+10^{-3}T^2-0.254T+12.72 \\ c=2\times10^{-12}T^5-4\times10^{-9}T^4+3\times10^{-6}T^3-10^{-3}T^2-0.124T-2.788 \\ d=-4\times10^{-9}T^4+8\times10^{-6}T^3+4\times10^{-3}T^2+0.69T+128.8 \\ e=-6\times10^{-14}T^5+10^{-10}T^4-10^{-7}T^3+3\times10^{-5}T^2-0.003T+0.151 \\ g=-2\times10^{-10}T^4+3\times10^{-7}T^3+0.0288T+0.893 \end{cases}$ | 0.9999 |
| F4 | $\begin{cases} a=-2\times10^{-11}T^5+5\times10^{-8}T^4-5\times10^{-5}T^3+1.7\times10^{-2}T^2-2.794T+142.0 \\ b=-9\times10^{-12}T^5-2\times10^{-8}T^4-2\times10^{-5}T^3+7\times10^{-3}T^2-1.239T+62.54 \\ c=7\times10^{-13}T^5-2\times10^{-9}T^4+10^{-6}T^3+0.039T+1.569 \\ d=-3\times10^{-9}T^5+5\times10^{-6}T^4-2\times10^{-6}T^3-2\times10^{-3}T^2-0.066T+151.6 \\ e=-5\times10^{-14}T^5+10^{-10}T^4-9\times10^{-8}T^3+3\times10^{-5}T^2+0.003T+0.116 \\ g=-2\times10^{-12}T^5+4\times10^{-9}T^4-3\times10^{-6}T^3-0.078T+1.641 \end{cases}$ | 0.9999 |

satisfactorily correlated with the experimental data collected between 29˚C and 950˚C.

Further investigations to functionally tie the constitutive behavior to the intrinsic constitution are expected by using of the machine learning or similar methods.

## Acknowledgments

The authors sincerely thank the Local Materials Promotion Authority

(MIPROMALO) in Cameroon for its collaboration in making available the samples used for this study. They equally express their gratitude to the National Civil Engineering Laboratory (LABOGENIE) in Cameroon and the Laboratoire de l'Unité de Recherche Argiles, Géochimie et Environnements sédimentaires (AGEs) de l'Université de Liège where all tests in this study were carried out.

## Conflicts of Interest

The authors declare no conflicts of interest regarding the publication of this paper.

## References

[1] Papayianni, J. and Valiasis, T. (1991) Residual Mechanical Properties of Heated Concrete Incorporating Different Pozzolanic Materials. *Materials and Structures*, **24**, 115-121. https://doi.org/10.1007/BF02472472

[2] Nassif, A.Y., Burley, E. and Rigden, S. (1995) A New Quantitative Method of Assessing Fire Damage to Concrete Structures. *Magazine of Concrete Research*, **47**, 271-278. https://doi.org/10.1680/macr.1995.47.172.271

[3] Wu, B., Ma, Z.C. and Ou, J.P. (1999) Experimental Research on Deformation and Constitutive Relationship of Concrete under Axial Loading and High Temperature. *Journal of Building Structures*, **20**, 42-49.

[4] Li, X.Y. and Bu, F.J. (2011) Residual Strength for Concrete after Exposure to High Temperatures. *International Conference*, *ICCIC* 2011, Wuhan, 17-18 September 2011, 382-390. https://doi.org/10.1007/978-3-642-23998-4_53

[5] Khaliq, W. and Kodur, V. (2012) High Temperature Mechanical Properties of High-Strength Fly Ash Concrete with and without Fibers. *ACI Materials Journal*, **109**, 665-674.

[6] Kodur, V.K.R., Kumar, P. and Rafi, M.M. (2020) Fire Hazard in Buildings: Review, Assessment and Strategies for Improving Fire Safety. *PSU Research Review*, **4**, 1-23. https://doi.org/10.1108/PRR-12-2018-0033

[7] Kodur, V.K.R. and Naser, M.Z. (2020) Structural Fire Engineering. McGraw-Hill Publication, London.

[8] Xie, Q.F., Zhang, L.P., Yin, S.H., *et al.* (2019) Effects of High Temperature on the Physical and Mechanical Properties of Carbonated Ordinary Concrete. *Advances in Materials Science and Engineering*, **2019**, Article ID: 5753232. https://doi.org/10.1155/2019/5753232

[9] Nishida, A. and Yamazaki, N. (1995) Study on the Properties of High Strength Concrete with Short Polypropylene Fiber for Spalling Resistance. In: *Proceedings of the International Conference on Concrete under Severe Conditions. CONSEC* 1995, E&FN Spon, London, 1141-1150.

[10] Kalifa, P., Menneteau, F.-D. and Quenard, D. (2000) Spalling and Pore Pressure in HPC at High Temperatures. *Cement and Concrete Research*, **30**, 1915-1927. https://doi.org/10.1016/S0008-8846(00)00384-7

[11] Kalifa, P., Chene, G. and Galle (2001) High-Temperature Behaviour of HPC with Polypropylene Fibers from Spalling to Microstructure. *Cement and Concrete Research*, **31**, 1487-1499. https://doi.org/10.1016/S0008-8846(01)00596-8

[12] Cheng, P., Kodur, V.K.R. and Wang, T.-C. (2004) Stress-Strain Curves for High Strength Concrete at Elevated Temperatures. *Journal of Materials in Civil Engi-*

*neering*, **16**, 84-90. https://doi.org/10.1061/(ASCE)0899-1561(2004)16:1(84)

[13] Khaliq, W. and Kodur, V. (2011) Thermal and Mechanical Properties of Fiber Reinforced High Performance Self-Consolidating Concrete at Elevated Temperatures. *Cement and Concrete Research*, **41**, 1112-1122. https://doi.org/10.1016/j.cemconres.2011.06.012

[14] Khaliq, W. and Khan, H.A. (2015) High Temperature Material Properties of Calcium Aluminate Cement Concrete. *Construction and Building Materials*, **94**, 475-487. https://doi.org/10.1016/j.conbuildmat.2015.07.023

[15] Zhang, H.-Y. Kodur, V., Cao, L. and Qi, S.-L. (2014) Fiber Reinforced Geopolymers for Fire Resistance Applications. *Procedia Engineering*, **71**, 153-158. https://doi.org/10.1016/j.proeng.2014.04.022

[16] Kodur, V. (2014) Properties of Concrete at Elevated Temperatures. *ISRN Civil Engineering*, **2014**, Article ID: 468510. https://doi.org/10.1155/2014/468510

[17] Khaliq, W. and Farrukh, B.M. (2016) High Temperature Mechanical and Material Properties of Burnt Masonry Bricks. *Materials and Structures*, **49**, 5195-5208. https://doi.org/10.1617/s11527-016-0854-0

[18] Gautam, P.K., Verma, A.K., Maheshwar, S. and Singh, T.N. (2016) Thermomechanical Analysis of Different Types of Sandstone at Elevated Temperature. *Rock Mechanics and Rock Engineering*, **49**, 1985-1993. https://doi.org/10.1007/s00603-015-0797-8

[19] Gautam, P.K., Verma, A.K., Maheshwar, S. and Singh, T.N. (2018) Effect of High Temperature on Physical and Mechanical Properties of Jalore Granite. *Journal of Applied Geophysics*, **159**, 460-474. https://doi.org/10.1016/j.jappgeo.2018.07.018

[20] Gautam, P.K., Verma, A.K., Maheshwar, S. and Singh, T.N. (2018) Evolution of Thermal Damage Threshold of Jalore Granite. *Rock Mechanics and Rock Engineering*, **51**, 2949-2956. https://doi.org/10.1007/s00603-018-1493-2

[21] Gautam, P.K., Verma, A.K., Hu, W. and Singh, T.N. (2019) Experimental Investigations on the Thermal Properties of Jalore Granitic Rocks for Nuclear Waste Repository. *Thermochimica Acta*, **681**, 178-381. https://doi.org/10.1016/j.tca.2019.178381

[22] Gautam, P.K., Jha, M.K., Verma, A.K. and Singh, T.N. (2019) Evolution of Absorption Energy per Unit Thickness of Damaged Sandstone. *Journal of Thermal Analysis and Calorimetry*, **136**, 2305-2318. https://doi.org/10.1007/s10973-018-7884-5

[23] Naser, M.Z. and Uppala, V. (2020) Properties and Material Models for Construction Materials Post Exposure to Elevated Temperatures. *Mechanics of Materials*, **142**, Article ID: 103293. https://doi.org/10.1016/j.mechmat.2019.103293

[24] Anupama, K.D., Priyadarsini, R.S. and Narayanan, S. (2021) High Temperature Effects on Different Grades of Concrete. *Sådhanå*, **46**, Article No. 31. https://doi.org/10.1007/s12046-020-01536-6

[25] Russo, S. and Sciarretta, F. (2013) Masonry Exposed to High Temperatures: Mechanical Behaviour and Properties—An Overview. *Fire Safety Journal*, **5**, 569-686. https://doi.org/10.1016/j.firesaf.2012.10.001

[26] Roudouane, H.T., Mbey, J.A., Bayiga, E.C. and Ndjigui, P.-D. (2020) Characterization and Application Tests of Kaolinite Clays from Aboudeia (Southeastern Chad) in Fired Bricks Making. *Scientific African*, **7**, e00294. https://doi.org/10.1016/j.sciaf.2020.e00294

[27] Onana, V.L., Ntouala, R.F.D., Mbey, J.A., Ngo'oZe, A., Kabeyene, V.K. and Eko-

deck, G.E. (2019) Mineralogy and Preliminary Assessment of the Potential Uses of Alluvial Clays from Batouri (Eastern-Cameroon). *Cerâmica*, **65**, 407-415. https://doi.org/10.1590/0366-69132019653752626

[28] Bidoung, J.C., Pliya, P., Meukam, P., Noumowé, A. and Beda, T. (2016) Behaviour of Clay Bricks from Small-Scale Production Units after High Temperature Exposure. *Materials and Structures*, **49**, 4991-5006. https://doi.org/10.1617/s11527-016-0838-0

[29] Hsu, L.S. and Hsu, C.-T. (1994) Stress-Strain Behaviour of Steel-Fiber High Strength Concrete under Compression. *Structural Journal*, **91**, 448-457. https://doi.org/10.1680/macr.1994.46.169.301

[30] Marco, A. and Mauro, S. (2011) Mechanical Behaviour of Full Unit Masonry Panels under Fire Action. *Fire Safety Journal*, **46**, 440-450. https://doi.org/10.1016/j.firesaf.2011.07.004

[31] Manita, P., Sideris, K.K. and Savva, A. (2005) Influence of Elevated Temperatures on the Mechanical Properties of Blended Cement Concretes Prepared with Limestone and Siliceous Aggregates. *Cement and Concrete Composites*, **27**, 239-248. https://doi.org/10.1016/j.cemconcomp.2004.02.013

[32] Ma, Q.M., Guo, R.X., Zhao, Z.M., Lin, Z.W. and He, K.H. (2015) Mechanical Properties of Concrete at High Temperature—A Review. *Construction and Building Materials*, **93**, 371-383. https://doi.org/10.1016/j.conbuildmat.2015.05.131

[33] Ercolani, G., Ortega, N.F., Priano, C. and Senas, L. (2017) Physical-Mechanical Behaviour of Concretes Exposed to High Temperatures and Different Cooling Systems. *Structural Concrete*, **18**, 487-495. https://doi.org/10.1002/suco.201500202

[34] Zeng, L., Ren, W.T. and Zou, Z.T. (2019) Experimental Study on Seismic Behaviour of Frame Structures Composed of Concrete Encased Columns with L-Shaped Steel Section and Steel Beams. *Earthquakes and Structures*, **16**, 97-107.

[35] Xiang, S., Zeng, L., Zhang, J., Chen, J., Liu, Y., Cheng, G. and Mo, J. (2019) A DIC-Based Study on Compressive Responses of Concrete after Exposure to Elevated Temperatures. *Materials*, **12**, Article No. 2044. https://doi.org/10.3390/ma12132044

[36] Mander, J.B., Priestley, M.J.N. and Park, R. (1988) Theoretical Stress-Strain Model for Confined Concrete. *Journal of Structural Engineering*, **114**, 1804-1825. https://doi.org/10.1061/(ASCE)0733-9445(1988)114:8(1804)

[37] Youssef, M.A. (2007) General Stress-Strain Relationship for Concrete at Elevated Temperatures. *Engineering Structures*, **29**, 2618-2634. https://doi.org/10.1016/j.engstruct.2007.01.002

[38] Mbumbia, L., Mertens de Wilmars, A. and Tirlocq, J. (2000) Performance Characteristics of Lateritic Soil Bricks Fired at Low Temperatures: A Case Study of Cameroon. *Construction and Building Materials*, **14**, 121-131. https://doi.org/10.1016/S0950-0618(00)00024-6

[39] Mbumbia, L. and Mertens de Wilmars, A. (2002) Behaviour of Low-Temperature Fired Laterite Bricks under Uniaxial Compressive Loading. *Construction and Building Materials*, **16**, 101-112. https://doi.org/10.1016/S0950-0618(01)00035-6

[40] Johari, I., Said, S., Hisham, B., Bakar, A. and Ahmad, Z.A. (2010) Effect of the Change of Firing Temperature on Microstructure and Physical Properties of Clay Bricks from Beruas (Malaysia). *Science of Sintering*, **42**, 245-254. https://doi.org/10.2298/SOS1002245J

[41] Li, N., Ma, X.F., Zhang, S.C., *et al.* (2020) Thermal Effects on the Physical and Mechanical Properties and Fracture Initiation of Laizhou Granite during Hydraulic Fracturing. *Rock Mechanics and Rock Engineering*, **53**, 2539-2556.

https://doi.org/10.1007/s00603-020-02082-7

[42] Russo, S. and Sciarretta, F. (2012) Experimental and Theoretical Investigation on Masonry after High Temperature Exposure. *Experimental Mechanics*, **52**, 341-359. https://doi.org/10.1007/s11340-011-9493-0

[43] NgonNgon, G.F., Yongue-Fouateu, R., Bitom, D.L. and Bilong, P. (2009) A Geological Study of Clayey Laterite and Clayey Hydromorphic Material of the Region of Yaoundé (Cameroon): A Prerequisite for Local Material Promotion. *Journal of African Earth Sciences*, **55**, 69-78. https://doi.org/10.1016/j.jafrearsci.2008.12.008

[44] Domingo, J.C. and Chu, K.-H. (1985) Stress-Strain Relationship for Plain Concrete in Compression. *Journal Proceedings*, **82**, 797-804.

[45] Eurocode 6 (2005) Design of Masonry Structures—Part 1-1: General Rules for Reinforced and Unreinforced Masonry Structures.

[46] Nguyen, Th.-D., Meftah, F., Chammas, R. and Mebarki, A. (2009) The Behaviour of Masonry Walls Subjected to Fire: Modelling and Parametric Studies in the Case of Hollow Burnt-Clay Bricks. *Fire Safety Journal*, **44**, 629-641. https://doi.org/10.1016/j.firesaf.2008.12.006

[47] Ying, C., Zhang, L., Xie, H., Liu, J., Liu, H. and Yang, B. (2019) Damage Ratio Based on Statistical Damage Constitutive Model for Rock. *Mathematical Problems in Engineering*, **2019**, Article ID: 3065414. https://doi.org/10.1155/2019/3065414

[48] Zhao, H., Wang, Y. and Liu, F.Q. (2017) Stress-Strain Relationship of Coarse RCA Concrete Exposed to Elevated Temperatures. *Magazine of Concrete Research*, **69**, 1-16.

## Nomenclature

$f_y$ = Stress at the yield point (MPa).

$\varepsilon_y$ = Strain at the yield point.

$f_b$ = Stress at the beginning of the linear zone (MPa).

$\varepsilon_b$ = Strain at the beginning of the linear zone.

$E$ = Linear modulus of elasticity (MPa).

$\beta$ = Material parameter that depends on the shape of the stress-strain curve.

$f_c'$ = Maximum stress.

$\varepsilon_c'$ = Strain corresponding to the maximum stress $f_c'$.

$E_{it}$ = Slope at the origin or initial tangent modulus.

$f_c$ = The maximum stress.

$a$ = Material parameter that depends on the shape of the stress-strain curve.

$b$ = Material parameter that depends on the shape of the stress-strain curve.

$c$ = Material parameter that depends on the shape of the stress-strain curve.

$d$ = Material parameter that depends on the shape of the stress-strain curve.

$e$ = Material parameter that depends on the shape of the stress-strain curve.

$g$ = Material parameter that depends on the shape of the stress-strain curve.

$\beta$ = Material parameter that depends on the shape of the stress-strain curve.

$\varepsilon_u$ = The maximum stress.

$T$ = Temperature T.

$E_{CT}$ = Compression modulus at temperature T.

$f_{CT}$ = The maximum stress at temperature T.